

Bone metabolic activity in hyperostosis cranialis interna measured with ^{18}F -fluoride PET

Jérôme J. Waterval · Thijs M. A. Van Dongen · Robert J. Stokroos · Jaap G. J. Teule · Gerrit J. Kemerink · Boudewijn Brans · Fred H. M. Nieman · Johannes J. Manni

Received: 24 July 2010 / Accepted: 19 October 2010 / Published online: 16 November 2010
© The Author(s) 2010. This article is published with open access at Springerlink.com

Abstract

Purpose ^{18}F -Fluoride PET/CT is a relatively undervalued diagnostic test to measure bone metabolism in bone diseases. Hyperostosis cranialis interna (HCI) is a (hereditary) bone disease characterised by endosteal hyperostosis and osteosclerosis of the skull and the skull base. Bone overgrowth causes entrapment and dysfunction of several cranial nerves. The aim of this study is to compare standardised uptake values (SUVs) at different sites in order to quantify bone metabolism in the affected anatomical regions in HCI patients.

Methods Nine affected family members, seven non-affected family members and nine non-HCI non-family members underwent ^{18}F -fluoride PET/CT scans. SUVs were systematically measured in the different regions of interest: frontal bone, sphenoid bone, petrous bone and clivus. Moreover, the average ^{18}F -fluoride uptake in the entire skull was measured by assessing the uptake in axial slides. Visual assessment of the PET scans of affected individuals was performed to discover the process of disturbed bone metabolism in HCI.

Results ^{18}F -Fluoride uptake is statistically significantly higher in the sphenoid bone and clivus regions of affected family members. Visual assessment of the scans of HCI patients is relevant in detecting disease severity and the pattern of disturbed bone metabolism throughout life.

Conclusion ^{18}F -Fluoride PET/CT is useful in quantifying the metabolic activity in HCI and provides information about the process of disturbed bone metabolism in this specific disorder. Limitations are a narrow window between normal and pathological activity and the influence of age. This study emphasises that ^{18}F -fluoride PET/CT may also be a promising diagnostic tool for other metabolic bone disorders, even those with an indolent course.

Keywords Bone dysplasias · Fluorine · Hyperostosis · Osteosclerosis · Positron emission tomography

Introduction

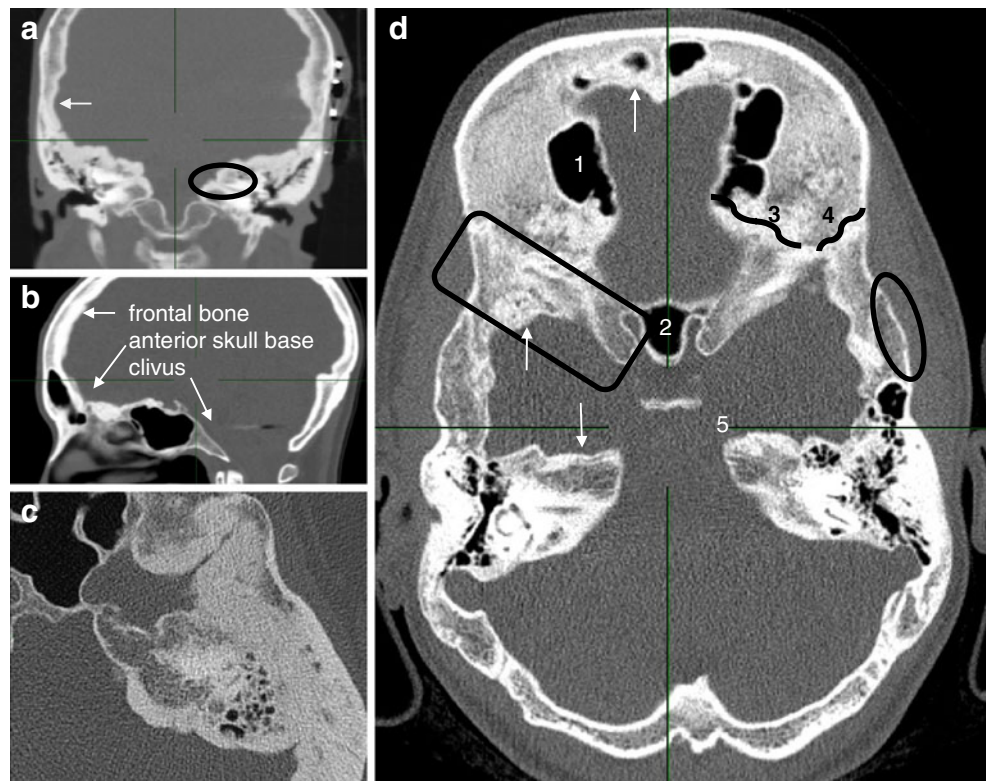
Hyperostosis cranialis interna (HCI) (Online Mendelian Inheritance in Man 144755) is a disorder which was first described in 1990 and is characterised by hyperostosis and osteosclerosis of the calvaria and skull base (Fig. 1) [1]. This leads to a narrowing of cranial nerve foramina causing entrapment and dysfunction of cranial nerves I, II, V, VII and VIII. Facial palsy and vestibulocochlear dysfunction occur at a young age, mainly in the second and third decades. Smell and vision impairment and trigeminal neuralgia may occur later. It is a hereditary disorder that, to date, has been diagnosed in three related Dutch families only [2]. Besides HCI, numerous bone dysplasias with skull base and calvarial hyperostosis and osteosclerosis exist. Van Buchem disease [3, 4], Camurati-Engelmann disease [5] and sclerosteosis [6] are examples of similar disorders

J. J. Waterval (✉) · T. M. A. Van Dongen · R. J. Stokroos · J. J. Manni
Department of Otorhinolaryngology and Head & Neck Surgery,
Maastricht University Medical Center,
P.O. 5800, 6202 AZ Maastricht, The Netherlands
e-mail: J.Waterval@gmail.com

J. G. J. Teule · G. J. Kemerink · B. Brans
Department of Nuclear Medicine,
Maastricht University Medical Center,
P.O. 5800, 6202 AZ Maastricht, The Netherlands

F. H. M. Nieman
Department of Clinical Epidemiology and Medical Technology
Assessment, Maastricht University Medical Center,
P.O. 5800, 6202 AZ Maastricht, The Netherlands

Fig. 1 CT images of affected individuals. **a** Coronal reconstruction of the middle skull base with near-total obliteration of the internal auditory canal (*oval*), endosteally thickened parietal area (*arrow*). Note the subcutaneous wires of auditory brainstem implantation device (*left*). **b** Paramedian sagittal reconstruction. Frontal bone and anterior skull base are affected. Vertebral column, nasal bones and clivus show no hyperostosis. **c** Axial image of the temporoparietal area revealing exorbitant endosteal hyperostosis. **d** Axial overview of a 24-year-old affected woman: 1 right frontal sinus, 2 sphenoid sinus, 3 sphenofrontal suture, 4 sphenoparietal suture, 5 apex of the left petrous bone. *Arrows* apposition of excessive endosteal bone. *Oval* normal configuration of outer cortex. *Square* sclerotic greater sphenoid wing



with increased bone density, however with metaphyseal and/or diaphyseal involvement. An overview of different (genetic) skeletal disorders is provided by the International Skeletal Dysplasia Society [7]. HCI is the only bone disorder affecting solely the skull.

The diagnosis of HCI is suspected by family history and physical examination and confirmed by computed tomography (CT). Analysis of sequential CT scans of affected individuals gives the impression that the frontal bone and the (medial part of the) petrous bone are affected first, in the late first or early second decade. This process seems to continue until the age of 40. In the greater sphenoid wing hyperdense areas are visible in adolescence (comparable to the frontal bone region); however, usually obvious hyperostosis starts later (third decade) and progresses until later in life. Findings for the parietal bone are similar, becoming pathologically dense and hyperostotic from the third decade on. The anterior and middle skull base are affected, whereas the occipital region is hardly involved (Fig. 1). In HCI there is no involvement of the tubular bones. An additional dynamic bone imaging technique, ^{18}F -fluoride positron emission tomography (PET), could provide valuable information in analysing and quantifying bone metabolism.

^{18}F -Fluoride was described as a tracer for bone imaging by Blau et al. in 1962 and 1972 (conventional scintigraphy), but fell into disuse [8, 9]. In 1992, PET scans using ^{18}F -fluoride were introduced to quantify bone formation

[10]. Compared to conventional gamma cameras including single photon emission computed tomography (SPECT), PET scans have higher spatial resolution and a greater sensitivity than gamma cameras and offer direct quantification of bone imaging studies. Grant et al. reviewed the available studies about clinical utility of ^{18}F -fluoride PET/CT scanning [11]. Although the specific bone uptake is similar for both radionuclides, there is less plasma protein binding of ^{18}F -fluoride [12] and the half-life is considerably shorter (110 min and 6 h, respectively). ^{18}F -Fluoride PET scanning offers shorter study times and is therefore more convenient for patient and physician. The effective dose of ^{18}F -fluoride PET is somewhat higher compared to $^{99\text{m}}\text{Tc}$ bone scanning (4.0 versus 3.0 mSv, respectively) [11]. ^{18}F -Fluoride PET is more accurate than planar imaging or SPECT with $^{99\text{m}}\text{Tc}$ -methylene diphosphonate (MDP) for the detection of small focal lesions, such as metastases [13]. Because of its easier quantification capabilities, ^{18}F -fluoride is very useful for the assessment of bone metabolism.

With ^{18}F -fluoride PET differences in bone metabolism between affected HCI patients, unaffected family members and unaffected control subjects are visualised and quantified in different anatomical subsites. The aims of this study are (1) to provide additional information about the early stage of HCI and (2) to monitor disease activity at different anatomical subsites and predict disease progression which can be important for treatment decisions.

Materials and methods

Subjects

The 3 related families have common progenitors and consist of 31 individuals (Fig. 2), 3 of whom are deceased. One individual did not participate because of a psychiatric condition at the time of the study. A total of 11 children (all under 5 years old) did not undergo a PET/CT scan because of their age. The remaining 16 were included: 9 family members with proven CT abnormalities (group 1) and 7 family members without CT abnormalities (group 2).

The control group consisted of nine patients (group 3), mainly examined for orthopaedic diagnostic reasons (without symptoms or a disease history in the head and neck region). The Medical Ethics Committee of the Maastricht University Medical Centre approved the research protocol (document number MUMC 09-4-050.4/PL) and all patients gave their written informed consent. All individuals underwent an ^{18}F -fluoride PET/CT scan between August 2007 and November 2008.

PET imaging

The average ^{18}F -fluoride activity administered to all patients was approximately 200 MBq (effective dose 5.4 mSv). PET/CT scans of the head and upper torso were made after 1 h, acquiring data for 4 min per bed position. A PET/CT scanner with a 64-slice CT component (Gemini TF, Philips, Best, The Netherlands) was used. In all cases, low-dose CT (30 mAs, 0.5 mSv) was performed. If needed for diagnostic reasons, high-resolution CT was performed as well. Using the standard Philips time-of-flight ordered

subsets expectation maximisation reconstruction (33 subsets, 3 iterations), images corrected for random events, scattered radiation and attenuation were obtained. The PET matrix size was 144, resulting in a voxel size of $4 \times 4 \times 4 \text{ mm}^3$.

Visual assessment

All PET scans were visually analysed and compared to the complementary CT scans with Philips Extended Brilliance™ Workspace in order to assess their clinical value. This programme is used for assessment of PET/CT scans in everyday clinical practice at our institute. The PET scans were fused with the 4-mm CT scans and depicted in “thermal” colour scale setting and compared to high-resolution CT scans of the skull base. The areas of interest were analysed by displaying identical settings: the low-level filter was set at standardised uptake value (SUV)=1.3 and the upper-level filter at SUV=12.0. Additionally, hot spots were detected by visual scoring of the scans and by assessing the SUV_{max} of each slice.

Standardised measurements

The scans were analysed using PMOD 2.95 (PMOD Technologies Ltd., Zurich, Switzerland). A region of interest (ROI) with a radius of 5 mm was placed in the axial plane around the maximal activity in different anatomical regions: greater sphenoid wing (left and right), frontal bone (cranial to orbital or frontal sinus), apex of the petrous bone (left and right) and clivus. Initially in each of these anatomical regions a manually drawn ROI was created including the entire region. This was repeated for all planes comprising the region concerned and in these ROIs the point of maximal activity was assessed. Conse-

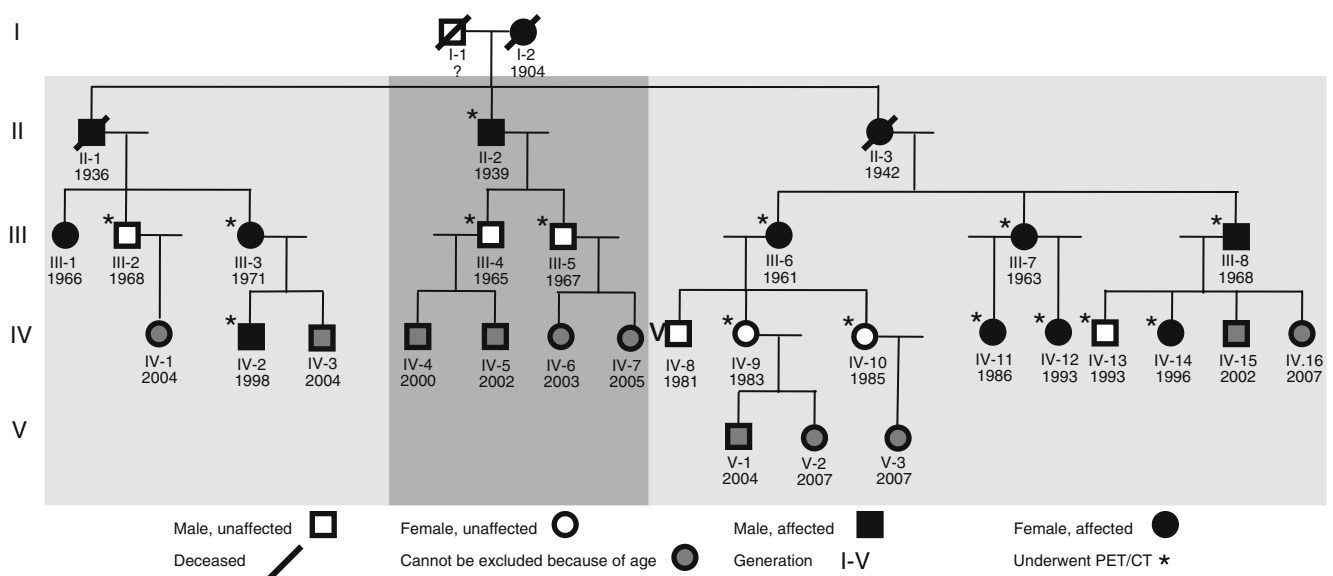


Fig. 2 Pedigree of the affected HCI families

quently, the coordinates of these points of maximal activity were used as the centre of the smaller, circular ROIs with a radius of 5 mm. The data of this ROI were used for calculation of the SUV. For all anatomical subsites the SUV_{mean} and SUV_{max} were calculated.

The corpus of the third cervical vertebra was chosen as internal control site. In the area scanned, the vertebrae, clavicles and the cheek bones are the only bony structures clearly not affected in HCI patients. The vertebrae were considered the most appropriate because of their size. None of the scanned individuals, regardless of group, had neck conditions.

Total uptake of the skull was also assessed. ROIs were created in the axial plane with the inside (A) and outside (B) boundaries of the skull (Fig. 3). The uptake in the bone was drawn up by subtracting the data of A from B. Next we calculated the average uptake in the entire skull. To accomplish this the average uptakes in all planes (from the skull base to the vertex) were added and divided by the total volume (slice thickness of one region equals 4 mm). With these data the SUVs of the ROIs were calculated using the following formula:

$$SUV[g/mL] = \frac{TissueActivity(kBq/mL)}{ActivityInjectedDose(kBq)/BodyWeight(g)}$$

Statistical analysis

Sample means, standard deviations and the range of SUV_{mean} and SUV_{max} were calculated per group.

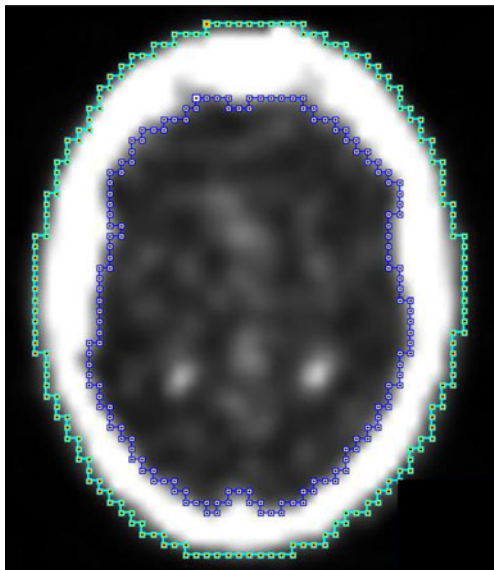


Fig. 3 Measuring the total uptake of the skull using PMOD 2.95: A (inside) = blue line, B (outside) = green line; total skull uptake per slice was calculated by subtracting the data of A from B (B–A). Results of all planes together (up from the skull base to the vertex) were added resulting in the total uptake of the bone

Kolmogorov-Smirnov tests were performed for all continuous metric data to test for normality. Frequencies and percentages are given for categorical data.

Both the parametric analysis of variance (ANOVA) and the nonparametric Kruskal-Wallis overall tests were performed to examine differences between the three groups. To compare HCI patients and non-HCI family members on the one hand and HCI patients and control subjects on the other hand, the parametric *t* test and the Mann-Whitney test were used.

All data were analysed with SPSS PC version 16; *p* values less than 0.05 were considered as denoting statistical significance.

Results

In group 1, nine (affected) individuals were included (six women and three men, mean age 32, range 11–68). Group 2 consisted of seven non-HCI family members (five women and two men, mean age 29, range 14–40). A total of nine control subjects (group 3) were scanned (five women and four men, mean age 60, range 42–75).

Visual assessment

General findings

Skull sutures show enhanced uptake in all individuals, both affected as well as unaffected. In unaffected individuals minor physiological irregularities are sometimes observed at the endosteal side of the frontal bone area on CT as well. However, other parts of the cranial vault are always smoothly delineated in unaffected individuals. Hot spots unrelated to HCI (Fig. 4) comprise among others areas of embryologically fused bone (i.e. clivus, sphenoid wing), the nasal bones and the temporomandibular joint.

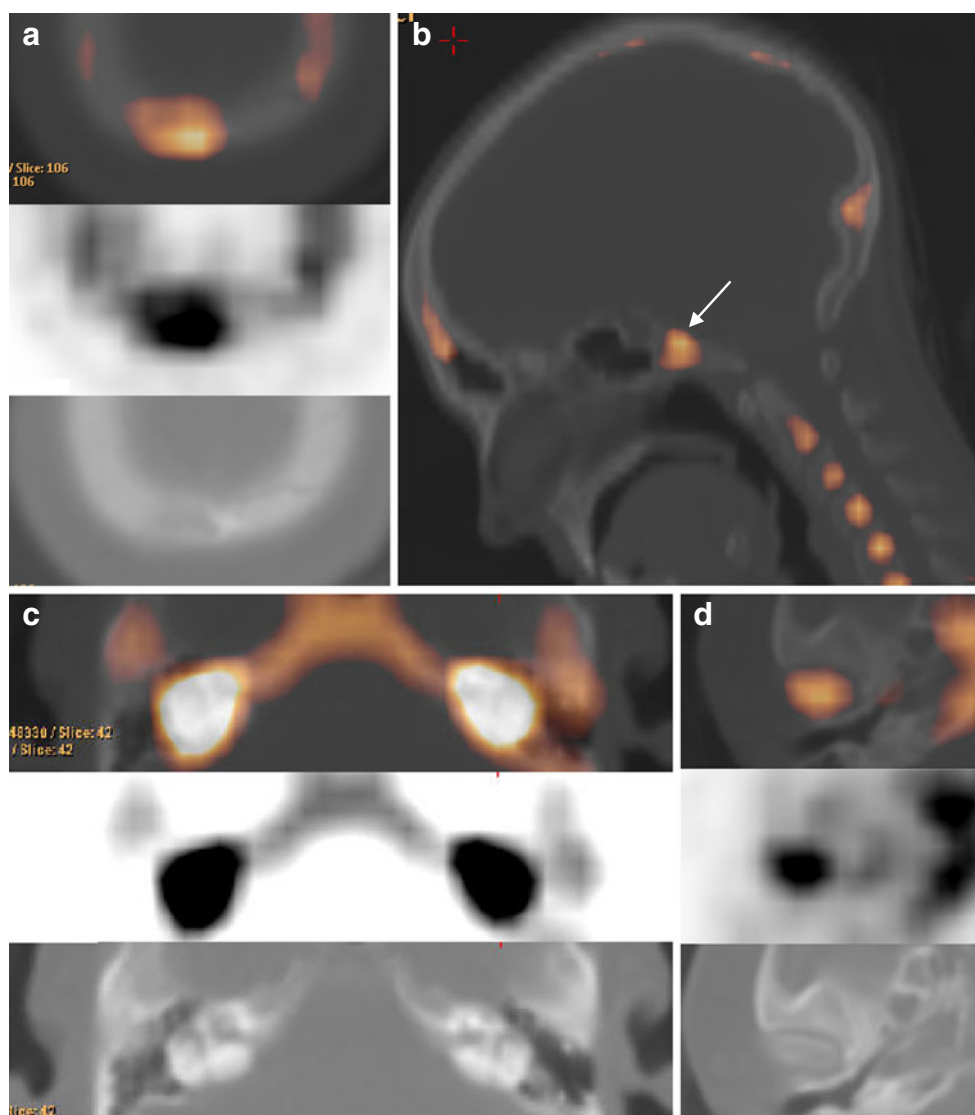
Hot spots and other interesting findings related to HCI are displayed in Fig. 5. The majority of the hot spots (besides those found in the standardised measurement areas) are found in three different regions: the cranial part of the frontal bone, the sphenofrontal suture and the occipital suture.

In HCI the first abnormal findings are seen in the frontal bone (Fig. 6). Generally, the endosteal abnormalities of the affected calvarial bones (frontal and parietal) are found at the base of the endosteal border of the hyperostotic region (Fig. 5c–f and Fig. 6).

Frontal bone area

The frontal bone area is a pathognomonic area in visual assessment. In young affected individuals (late first, early second decade), a typical enhancement pattern is observed (Fig. 6). First subtle sclerotic changes of the skull are

Fig. 4 Hot spots unrelated to HCI. **a** Occipital osteoma cranial to the foramen magnum. **b** Hot spots visible in metabolically active bone regions. Note the clivus (*arrow*), which is a junction of two bone segments. The centre of the corpora of the vertebral column and the occipital protuberance show enhanced activity as well. **c** Bilateral enhancement of the labyrinth in a control subject with cochlear otosclerosis. **d** Hot spot at the caput mandibulae/temporomandibular joint



observed (CT). When abnormalities on CT are hardly visible, frontal endosteal activity is detected (Fig. 6a). Hot spots are seen at sclerotic sites and diffusely enhanced areas are seen at (CT) hypodense hyperostotic areas. Frontal bone uptake gradually becomes more explicit during the second decade and can become fulminant (Fig. 6b). As soon as an endosteal border of bone apposition is visible, the abnormal activity is observed at the endosteal side of the diploë (bone marrow) and not centrally in the endosteal border (Fig. 6b, c). Later (>30 years), frontal bone activity gradually decreases and the process of hyperostosis extinguishes (Fig. 6d, e).

Petrous bone area

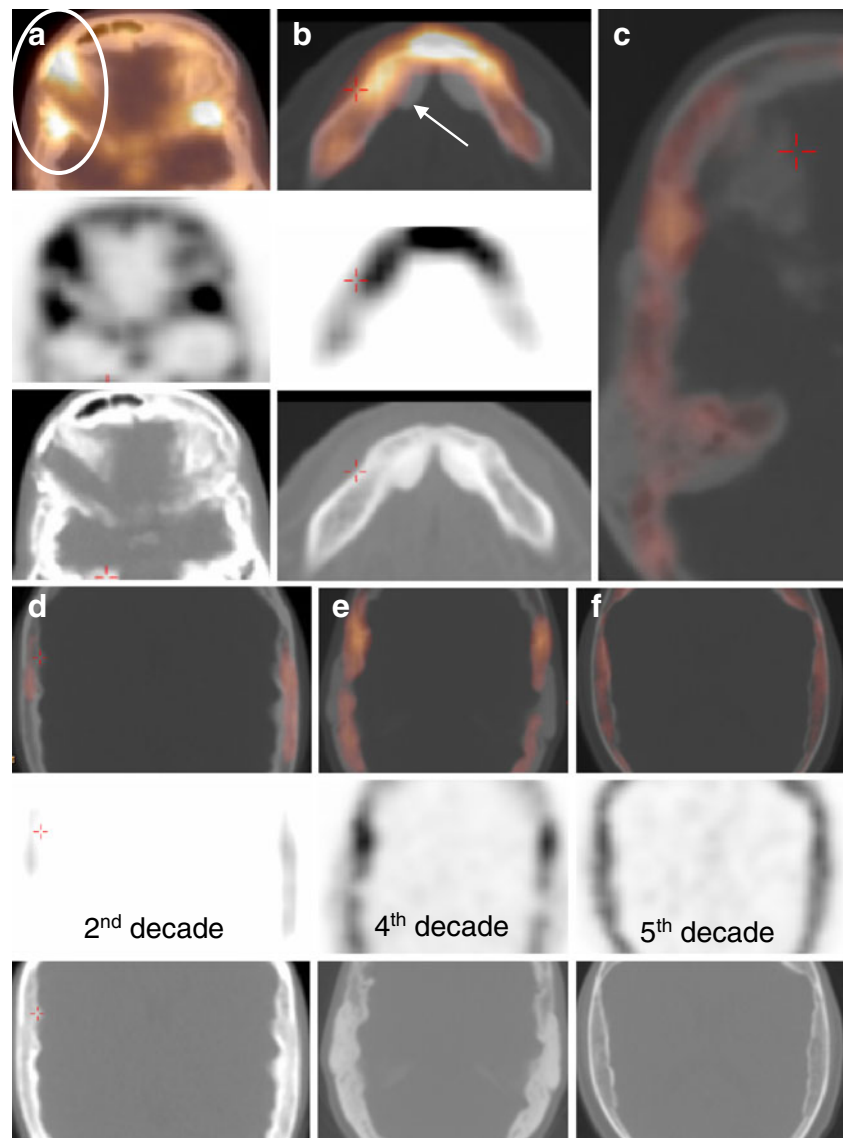
A varying inter-individual degree of pneumatization and increasing pneumatization throughout life make it difficult to precisely quantify bone metabolism in this region. Therefore, visual assessment of the scans of HCI patients is

important in that it shows a typical enhancement pattern. Affected adolescents and patients in their 20s have diffuse enhancement of the petrous bone apex in the region of the internal auditory canal (Fig. 7a, b), representing active osteosclerosis and hyperostosis of the medial part of the petrous bone (the region around the internal auditory canal containing the facial and vestibulocochlear nerves). From the age of 30 onward the typical endosteal enhancement pattern can be recognised as earlier in the frontal area (Fig. 7c, d). There is a diffuse hyperactive border at both the anterior and posterior side of the petrous bone, the latter vanishing with increasing age (Fig. 7e). Throughout life, there is no disease involvement of the mastoid, middle and inner ear visible with ^{18}F -fluoride PET, corresponding to the CT findings.

Sphenoid bone and temporal area

At the sites of fusion of the great wing of the sphenoid bone and the temporal and frontal bone (sphenopetrosal and spheno-

Fig. 5 Hot spots and other findings in HCI-affected individuals. **a** Postoperative status after optic nerve decompression at the right side in an affected individual. The oblique operation tract can still be seen (*oval*). Hot spot at the junction between the greater sphenoid wing, the frontal bone and the parietal bone at the left side. **b** Hot spot at the symphysis mandibulae. Typically the mandibular exostoses (*arrow*) do not show enhanced uptake; the symphysis mandibulae and the base of the exostoses do have enhanced uptake. **c** View of the whole right axial skull base of a 39-year-old woman. Note that the activity is located at the base of the endosteal border of the hyperostosis. **d–f** Enhanced activity of the parietal area. Note that the activity is not located in the endosteal part solely, but mainly at the base of the hyperostotic border



frontal suture) there is enhancement in both affected as well as unaffected individuals. No typical pattern is visible in the abnormalities of the sphenoid bone area. Affected individuals have more pronounced activity at the surrounding endosteal part of the greater sphenoid wing. During life, an impressive endosteal border of additional bone forms at the level of the greater sphenoid wing and parietal bone, which remains more active than the sphenoid area in healthy individuals.

Data analysis

The results of the standard measurements for all groups together are shown in Table 1. Table 2 shows a breakdown of SUV parameters per group. The average SUV seems to be higher in group 1 for all locations except for the control site of the third cervical vertebra.

The average SUV of the *complete skull* is not significantly higher for group 1 ($SUV=1.74\pm 0.55$) when compared to groups 2 and 3 (1.49 ± 0.21 and 1.44 ± 0.55).

Uptake of ^{18}F -fluoride in the *frontal region* (SUV_{mean}) is higher in the HCI group but no statistical significance is reached (ANOVA $p=0.06$, Kruskal-Wallis $p=0.14$). To investigate whether the outcomes were dependent on age, patients above and below the age of 40 were compared and on average the younger group had a 1.63 higher value, this difference being just barely statistically significant for the ANOVA ($p=0.049$) and not quite for the Kruskal-Wallis test ($p=0.051$).

The group average SUV_{mean} in the *petrous bone region* is higher in HCI patients as compared to the other groups (group 1 4.47 ± 1.56 versus group 2 3.93 ± 1.31 and group 3 3.82 ± 0.96), but not statistically significant.

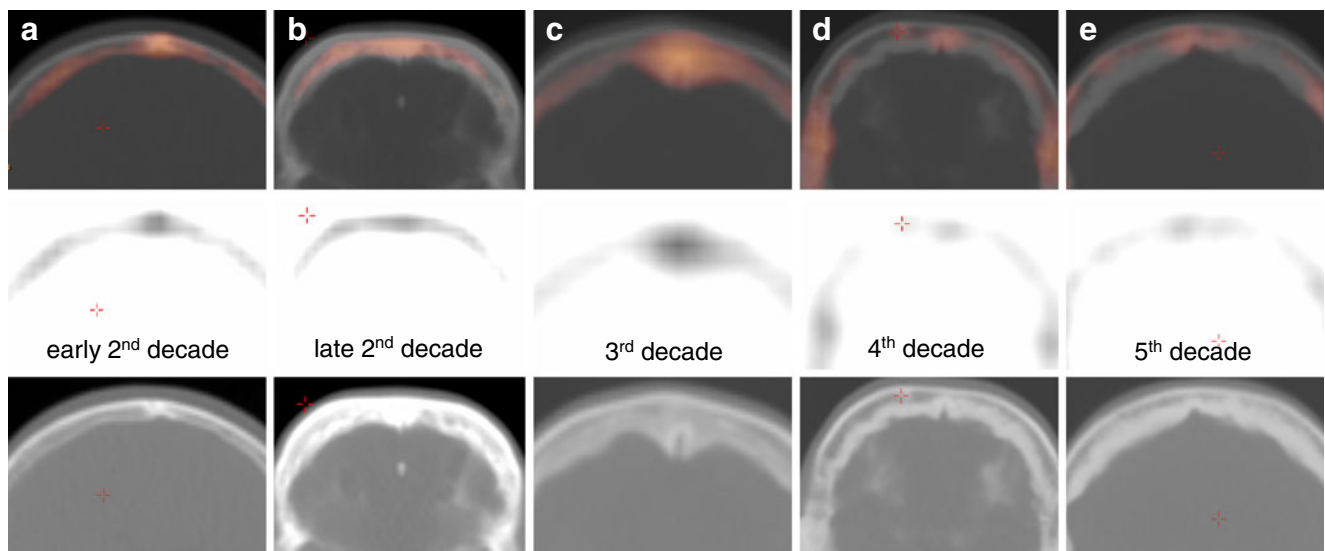


Fig. 6 a–e Evolution of the disturbed bone metabolism throughout life in HCI patients, as observed in the frontal bone area. Note that the outer cortex is not abnormal; however, the endosteal border thickens during life and the enhanced activity is found at the base of the hyperostotic border

The *clivus* and the *sphenoid bone* regions have corresponding findings, although the sphenoid area is affected by HCI and the clivus does not show obvious hyperostosis. SUV_{mean} in the clivus area is 6.17 ± 1.38 in group 1, 5.70 ± 1.36 in group 2 and 4.18 ± 1.12 in group 3. There is a statistical significance between group 1 and group 3 for both SUV_{mean} and SUV_{max} (t test $p=0.010$ and rank test $p=0.009$). SUV_{mean} in the sphenoid area is 6.58 ± 1.62 in group 1, 5.66 ± 1.21 in group 2 and 7.75 ± 2.03 in group 3. SUV_{max} values show comparable results. In both areas age seems to influence the SUV values: group 2 values are positioned in between groups 1 and 3, 1 being the highest (with youngest average age) and 3 the lowest

(with highest average age). For the sphenoid area a statistically significant difference between groups 2 and 3 is also found.

In Table 3 the SUV values of the hot spots in HCI patients are displayed.

Discussion

Technical considerations concerning ^{18}F -fluoride PET/CT

To obtain reproducible outcome measurements several pharmacokinetic models have been described for ^{18}F -

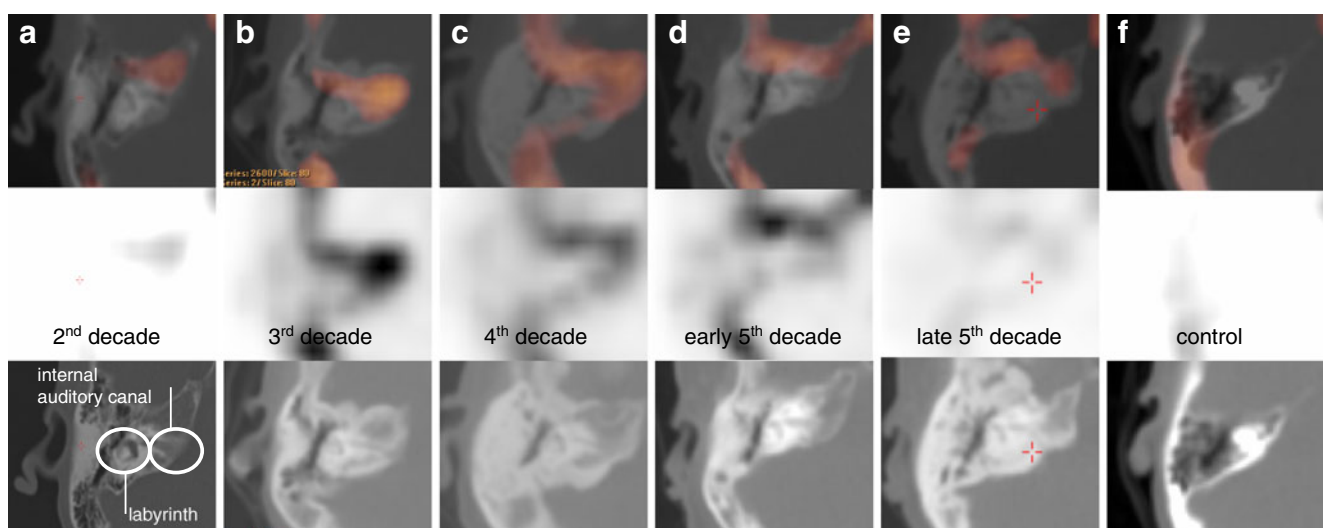


Fig. 7 a–f Bone metabolic activity of the petrous bone throughout life. There is important enhanced activity in the inner auditory canal region, corresponding to the facial and vestibulocochlear nerve impingement. Note the absence of enhancement in the control subject (age 29)

Table 1 Descriptive statistics for SUV_{mean} and SUV_{max} for all locations and all individuals (n=25)

| Location | Mean SUV _{mean} | SD | Range | Mean SUV _{max} | SD | Range |
|-------------------------|--------------------------|------|------------|-------------------------|------|------------|
| Total uptake | 1.56 | 0.48 | 0.83–2.62 | - | - | - |
| Frontal bone | 3.67 | 1.34 | 1.91–7.50 | 4.33 | 1.53 | 2.33–8.59 |
| Clivus | 5.32 | 1.52 | 2.49–8.75 | 6.01 | 1.77 | 2.87–9.85 |
| Petrous bone(L&R) | 4.09 | 1.35 | 1.86–8.27 | 4.86 | 1.55 | 2.09–9.41 |
| Sphenoid bone (L&R) | 5.50 | 1.74 | 2.80–11.82 | 6.21 | 2.01 | 3.34–13.77 |
| Third cervical vertebra | 7.83 | 2.34 | 4.09–15.42 | 8.79 | 2.65 | 4.50–17.76 |

SD standard deviation, L&R average of left and right

fluoride PET scans. Hawkins et al. developed a three-compartment model producing quantitative measurements for the net uptake of ¹⁸F-fluoride into bone [10]. A rate constant (K) for this uptake can be calculated as a macro-parameter using the individual rate constants described in the model obtained by nonlinear regression methods (NLR). This K_{NLR} provides a tool for measuring the bone turnover that correlates with biochemical data and bone histomorphometric analyses performed on biopsy samples [14, 15]. However, it requires blood sampling and is therefore not widely used in clinical practice. Brenner et al. recognised this and compared the K_{NLR} to the more commonly used SUV for semi-quantitative metabolic bone measurements [16]. They found a strong positive linear correlation that was highly significant and reproducible. Thus, SUV is not only more practical and noninvasive but also equally reliable using ¹⁸F-fluoride in PET imaging. Installé et al. confirmed this after comparing kinetic modelling, SUV and biochemical markers in monitoring the therapeutic response in Paget’s disease of bone [17]. This study confirms the reproducibility of SUV in both unaffected as well as affected regions.

Standardised measurements of ¹⁸F-fluoride uptake in HCl compared to healthy controls and non-affected family members

We analysed SUV_{max} and SUV_{mean} at different anatomical locations following a structured protocol. Both outcome measures give comparable results. Statistical power was limited by the small group sizes. Uptake in the third cervical vertebra served well as an internal control measurement. Statistically significant differences were found for various measurements of the sphenoid bone and clivus. With respect to the frontal measurement there is clearly a tendency, however missing power in the statistical analysis.

No significant differences were seen between the groups concerning the *total uptake of the skull*. A plausible explanation is the inclusion of normal bone tissue (the outer part of the skull) in group 1 within the ROIs, averaging the scores. Measuring total uptake was time-consuming and considering the results obtained it does not appear to be an efficient contribution.

Uptake in the *frontal bone* showed nearly statistically significant differences between the study groups. We did

Table 2 SUV_{mean} and SUV_{max} for all bone locations for each of the different groups studied (n=25)

| Location | SUV | Group | | | p value | |
|-------------------------|------|---------------------------|-------------------------|------------------------------|---------|----------------|
| | | 1 (n=9), HCl | 2 (n=7), family non-HCl | 3 (n=9), control | ANOVA | Kruskal-Wallis |
| Total uptake | Mean | 1.74±0.55 | 1.49±0.21 | 1.44±0.55 | 0.412 | 0.427 |
| Frontal bone | Mean | 4.51±1.65 | 3.17±0.87 | 3.23±0.94 | 0.060 | 0.140 |
| | max | 5.22±1.87 | 3.78±1.07 | 3.87±1.13 | 0.090 | 0.136 |
| Clivus | Mean | 6.17±1.38 ^{a, b} | 5.70±1.36 | 4.18±1.12 ^{a, b} | 0.010 | 0.016 |
| | max | 7.00±1.61 ^{a, b} | 6.43±1.70 | 4.70±1.22 ^{a, b} | 0.011 | 0.023 |
| Petrous bone | max | 4.47±1.56 ^a | 3.93±1.31 | 3.82±0.96 | 0.534 | 0.542 |
| | Mean | 5.36±1.61 | 4.67±1.64 | 4.52±1.19 | 0.461 | 0.488 |
| Sphenoid bone | Mean | 6.58±1.62 ^{a, c} | 5.66±1.21 ^b | 4.30±0.93 ^{a, b, c} | 0.004 | 0.007 |
| | max | 7.48±1.88 ^{a, c} | 6.36±1.29 ^b | 4.82±0.97 ^{a, b, c} | 0.003 | 0.006 |
| Third cervical vertebra | Mean | 7.28±1.71 | 8.18±2.22 | 8.09±3.05 | 0.701 | 0.859 |
| | max | 8.17±1.93 | 9.12±2.36 | 9.16±3.54 | 0.693 | 0.873 |

^a Significantly different, p≤0.01 (Bonferroni t test)

^{b, c} Significantly different, p≤0.01 (Mann-Whitney)

Table 3 Hot spots found in HCI patients

| Location | SUV _{mean} | SUV _{max} |
|--------------------------|---------------------|--------------------|
| Frontal bone, skull base | 6.49 | 7.25 |
| | 7.78 | 9.47 |
| | 8.60 | 9.85 |
| | 8.68 | 9.94 |
| | 9.24 | 10.69 |
| | 11.94 | 13.63 |
| | 12.91 | 15.61 |
| Frontal bone, skullcap | 4.77 | 6.45 |
| | 7.57 | 8.78 |
| | 7.82 | 9.09 |
| | 12.44 | 13.73 |
| Occipital suture | 7.40 | 8.82 |
| | 7.59 | 9.05 |
| | 8.03 | 9.24 |
| | 8.74 ^a | 11.24 ^a |
| | 9.09 ^a | 11.71 ^a |

The paired SUV_{mean} and SUV_{max} represent one hot spot in one patient

^aResults from the same patient

expect this difference because this part of the skull base and skullcap is unequivocally affected in patients and abnormalities develop especially in the first decades. The findings do encourage our hypothesis that in the frontal area the process of hyperostosis and osteosclerosis peaks in the first decades of life and settles down thereafter. Typically there is no difference between groups 2 and 3, regardless of the unequal age distribution.

The higher uptake of ¹⁸F-fluoride in the *petrous bone* of HCI patients does correspond with our expectations, because the temporal bone is an affected region. Although the average uptake is higher in group 1 compared to groups 2 and 3, this difference was not statistically significant. Different degrees of pneumatization are encountered and cannot be corrected for in this area. Another explanation, which becomes clear after visually studying the PET and CT scans, is the fact that the affected region of the petrous bone is confined to the endosteal border only.

Uptake in the *clivus and sphenoid region* are both significantly higher for the patients compared to the control group as well as compared to the family non-HCI group. The mean uptake values of unaffected family members are obvious between groups 1 and 3 and this demands explanation. As opposed to other sites, these anatomical regions have in common that they are active growth centres (skull base sutures), explaining an increased local fluoride uptake in bone tissue representing osteoblastic activity [18, 19]. Increasing age is accompanied by a reduction of standard bone activity in these anatomical areas [20].

Value of visual assessment in HCI

¹⁸F-Fluoride PET is a very sensitive imaging technique. Hot spots are found long after surgical interventions (mastoidectomy, optic nerve decompression) and after facial trauma (nasal and cheek bones). Also, larger regions with a diffusely increased uptake are not necessarily pathological. Craniofacial sutures and growth centres (such as the clivus) have diffusely enhanced ¹⁸F-fluoride uptake, congruent to the objective measurements.

PET activity in the petrous bone region is confirmed by clinical findings. Facial nerve palsy and vestibulocochlear nerve impairment generally occur in the first 30 years of life due to impingement of the nerve at the level of the internal auditory canal, where increased PET activity is then observed. Along with the lifetime progression of hyperostosis, one would expect progression to total facial paralysis and deafness. Typically, the PET activity in this region surrounding the internal auditory canal decreases, explaining why the clinical symptomatology remains stable (Fig. 7).

Clinical application of ¹⁸F-fluoride PET/CT for HCI and bone metabolic disorders in general

In studies using ¹⁸F-fluoride there is limited experience with SUV in spite of the advantages and proven reliability [16, 17]. Uchida et al. demonstrated differences in SUVs in the lumbar spine after alendronate treatment in osteoporosis patients [21]. Reference SUV scores of different areas of normal bone with this tracer are scarcely described in the literature. No other studies were found with a detailed description of average uptake values of unaffected bone in different anatomical sites.

CT scanning will remain the gold standard for the diagnosis of HCI because of its high resolution. However, there is a need to quantify the disease activity rather than to perform sequential CT scans. This study confirms that ¹⁸F-fluoride PET/CT is a very sensitive imaging technique in determining disease activity, showing differences in small population sizes. The indolent character of this metabolic disorder raises an important limitation: there is a narrow window between normal and pathological metabolic activity. Therefore, SUV measurements should always be accompanied with the visual interpretation of changing bone activity patterns over time in different regions.

Age is the most important covariate to take into account in regions with a high bone turnover (i.e. sphenoid and clivus area) as osteoblastic activity diminishes with increasing age resulting in a lower uptake of ¹⁸F-fluoride [20]. In this study we had difficulties finding young individuals to serve as appropriate control subjects. This caused an unequal age distribution in the different groups and was

therefore potentially one of the most serious drawbacks of this study. To overcome this, group 2 (non-affected family members) with a similar age distribution as group 1 served as a secondary control group and showed similar results as group 3.

This study uses the semi-quantitative SUV ratio for the first time in a case-control study. The use of a consistent internal control site is important as an internal validation check of correct SUV processing. ^{18}F -Fluoride PET/CT, analysed by SUV, appears to be reliable since we found differences supporting our hypotheses. If the aforementioned limitations are taken into account, the combination of SUV measurements and visual interpretation can be of important value and might bring ^{18}F -fluoride PET/CT closer to being a diagnostic test for metabolic bone diseases.

Conflicts of interest None.

Open Access This article is distributed under the terms of the Creative Commons Attribution Noncommercial License which permits any noncommercial use, distribution, and reproduction in any medium, provided the original author(s) and source are credited.

References

- Manni JJ, Scaf JJ, Huygen PL, Cruysberg JR, Verhagen WI. Hyperostosis cranialis interna. A new hereditary syndrome with cranial-nerve entrapment. *N Engl J Med* 1990;322:450–4.
- Waterval JJ, Stokroos RJ, Bauer NJ, De Bondt RB, Manni JJ. Phenotypic manifestations and management of hyperostosis cranialis interna, a hereditary bone dysplasia affecting the calvaria and the skull base. *Am J Med Genet A* 2010;152A:547–55.
- Beighton P, Barnard A, Hamersma H, van der Wouden A. The syndromic status of sclerosteosis and van Buchem disease. *Clin Genet* 1984;25:175–81.
- Vanhoenacker FM, Balemans W, Tan GJ, Dikkers FG, De Schepper AM, Mathysen DG, et al. Van Buchem disease: lifetime evolution of radioclinical features. *Skeletal Radiol* 2003;32:708–18.
- Janssens K, Vanhoenacker F, Bonduelle M, Verbruggen L, Van Maldergem L, Ralston S, et al. Camurati-Engelmann disease: review of the clinical, radiological, and molecular data of 24 families and implications for diagnosis and treatment. *J Med Genet* 2006;43:1–11.
- Hamersma H, Gardner J, Beighton P. The natural history of sclerosteosis. *Clin Genet* 2003;63:192–7.
- Superti-Furga A, Unger S. Nosology and classification of genetic skeletal disorders: 2006 revision. *Am J Med Genet A* 2007;143:1–18.
- Blau M, Ganatra R, Bender MA. ^{18}F -fluoride for bone imaging. *Semin Nucl Med* 1972;2:31–7.
- Blau M, Nagler W, Bender MA. Fluorine-18: a new isotope for bone scanning. *J Nucl Med* 1962;3:332–4.
- Hawkins RA, Choi Y, Huang SC, Hoh CK, Dahlbom M, Schiepers C, et al. Evaluation of the skeletal kinetics of fluorine-18-fluoride ion with PET. *J Nucl Med* 1992;33:633–42.
- Grant FD, Fahey FH, Packard AB, Davis RT, Alavi A, Treves ST. Skeletal PET with ^{18}F -fluoride: applying new technology to an old tracer. *J Nucl Med* 2008;49:68–78.
- Blake GM, Park-Holohan SJ, Cook GJ, Fogelman I. Quantitative studies of bone with the use of ^{18}F -fluoride and $^{99\text{m}}\text{Tc}$ -methylene diphosphonate. *Semin Nucl Med* 2001;31:28–49.
- Even-Sapir E, Metser U, Mishani E, Lievshitz G, Lerman H, Leibovitch I. The detection of bone metastases in patients with high-risk prostate cancer: $^{99\text{m}}\text{Tc}$ -MDP planar bone scintigraphy, single- and multi-field-of-view SPECT, ^{18}F -fluoride PET, and ^{18}F -fluoride PET/CT. *J Nucl Med* 2006;47:287–97.
- Messa C, Goodman WG, Hoh CK, Choi Y, Nissenson AR, Salusky IB, et al. Bone metabolic activity measured with positron emission tomography and [^{18}F]fluoride ion in renal osteodystrophy: correlation with bone histomorphometry. *J Clin Endocrinol Metab* 1993;77:949–55.
- Piert M, Zittel TT, Becker GA, Jahn M, Stahlschmidt A, Maier G, et al. Assessment of porcine bone metabolism by dynamic [^{18}F] fluoride ion PET: correlation with bone histomorphometry. *J Nucl Med* 2001;42:1091–100.
- Brenner W, Vernon C, Muzi M, Mankoff DA, Link JM, Conrad EU, et al. Comparison of different quantitative approaches to ^{18}F -fluoride PET scans. *J Nucl Med* 2004;45:1493–500.
- Installé J, Nzeusseu A, Bol A, Depresseux G, Devogelaer JP, Lonneux M. (^{18}F)-fluoride PET for monitoring therapeutic response in Paget's disease of bone. *J Nucl Med* 2005;46:1650–8.
- Ishiguro K, Nakagaki H, Tsuboi S, Narita N, Kato K, Li J, et al. Distribution of fluoride in cortical bone of human rib. *Calcif Tissue Int* 1993;52:278–82.
- Narita N, Kato K, Nakagaki H, Ohno N, Kameyama Y, Weatherell JA. Distribution of fluoride concentration in the rat's bone. *Calcif Tissue Int* 1990;46:200–4.
- Chan GK, Duque G. Age-related bone loss: old bone, new facts. *Gerontology* 2002;48:62–71.
- Uchida K, Nakajima H, Miyazaki T, Yayama T, Kawahara H, Kobayashi S, et al. Effects of alendronate on bone metabolism in glucocorticoid-induced osteoporosis measured by ^{18}F -fluoride PET: a prospective study. *J Nucl Med* 2009;50:1808–14.